Symmetrical dynamics of peak current-mode and valley current-mode controlled switching dc–dc converters with ramp compensation*

Zhou Guo-Hua(周国华)[a)†], Xu Jian-Ping(许建平)[a)],
Bao Bo-Cheng(包伯成)[b)], and Jin Yan-Yan(金艳艳)[a)]

[a)] *School of Electrical Engineering, Southwest Jiaotong University, Chengdu* 610031, *China*
[b)] *School of Electrical and Information Engineering, Jiangsu Teachers University of Technology, Changzhou* 213001, *China*

(Received 6 November 2009; revised manuscript received 8 December 2009)

The discrete iterative map models of peak current-mode (PCM) and valley current-mode (VCM) controlled buck converters, boost converters, and buck–boost converters with ramp compensation are established and their dynamical behaviours are investigated by using the operation region, parameter space map, bifurcation diagram, and Lyapunov exponent spectrum. The research results indicate that ramp compensation extends the stable operation range of the PCM controlled switching dc–dc converter to $D > 0.5$ and that of the VCM controlled switching dc–dc converter to $D < 0.5$. Compared with PCM controlled switching dc–dc converters with ramp compensation, VCM controlled switching dc–dc converters with ramp compensation exhibit interesting symmetrical dynamics. Experimental results are given to verify the analysis results in this paper.

Keywords: discrete iterative map model, dynamics, switching converters, ramp compensation
PACC: 0545

1. Introduction

Switching dc–dc converters are strongly nonlinear circuits with rich nonlinear phenomena, such as low-frequency oscillation,[1−3] period-doubling bifurcation,[4−7] border collision bifurcation,[8−11] Hopf bifurcation,[12,13] time bifurcation,[14] complex intermittency and chaos,[15,16] and so on. With the variation of circuit parameters, switching dc–dc converters will enter into chaos via various bifurcations, which has a great effect on their performance. Therefore, dynamical behaviours and nonlinear phenomena of switching dc–dc converters have been investigated extensively in recent years.

The current-mode control technique is one of the most widely applied control techniques for switching dc–dc converters. A lot of research work has been done on the nonlinear phenomena and dynamical behaviours of switching dc–dc converters with peak current-mode (PCM) control.[7,10,12,17−21] Recently, the nonlinear phenomena and dynamical behaviours of switching dc–dc converters, operating in a continuous conduction mode (CCM), with valley current-mode (VCM) control have been reported by establishing two-dimensional and one-dimensional discrete iterative map models.[22,23]

PCM control and VCM control are two different control techniques with different application areas. It is known that by using ramp compensation, PCM controlled switching dc–dc converters can shift from discontinuous conduction mode (DCM) to CCM and effectively operate in a stable period-one region,[9,10] while VCM controlled switching dc–dc converters can operate only in CCM.[22]

In the present paper, we mainly focus on the study of dynamical behaviours of VCM controlled switching dc–dc converters operating in CCM with ramp compensation, and illustrate how the slope of the compensation ramp affects the dynamical behaviour and operation region of a switching dc–dc converter. The operation region, parameter space map, bifurcation diagram, and Lyapunov exponent spec-

*Project supported by the National Natural Science Foundation of China (Grant No. 50677056), the Natural Science Foundation of Jiangsu Province, China (Grant No. BK2009105), the Cultivation Project of Excellent Doctorate Dissertation of Southwest Jiaotong University, China, and the Doctoral Innovation Foundation of Southwest Jiaotong University, China.

†Corresponding author. E-mail: ghzhou-swjtu@163.com

© 2010 Chinese Physical Society and IOP Publishing Ltd

trum of three basic switching dc–dc converters (buck, boost, and buck-boost) are investigated in detail.

2. Iterative map models with ramp compensation

Figure 1 shows PCM and VCM controlled buck converters with ramp compensation, where $I_{\rm pk}$ and $I_{\rm vy}$ are the peak and the valley reference current respectively, $m_{\rm c}$ is the slope of the compensation ramp, $i_{\rm pk}$ and $i_{\rm vy}$ are the compensated peak and the compensated valley reference current, respectively, given by

$$i_{\rm pk} = I_{\rm pk} - m_{\rm c}(t \bmod T), \tag{1a}$$

$$i_{\rm vy} = I_{\rm vy} + m_{\rm c}(t \bmod T), \tag{1b}$$

where T is the clock period and $(t \bmod T)$ is t modulo T.

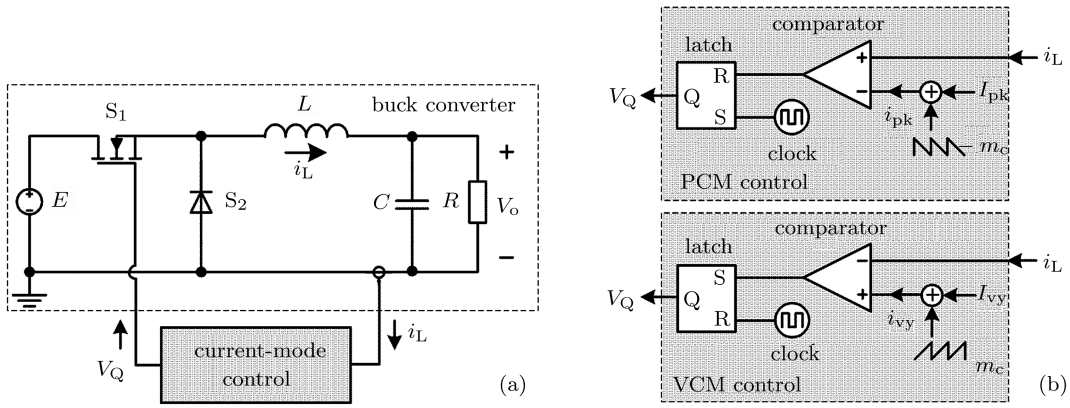


Fig. 1. PCM and VCM controlled buck converters with ramp compensation. Panel (a) shows their power state and panel (b) exhibits their control circuits.

For the PCM control, power switch S_1 turns on at the beginning of each switching cycle, turns off when the inductor current $i_{\rm L}$ increases to $i_{\rm pk}$, and remains in an off-state until the end of the present switching cycle. For the VCM control, switch S_1 turns off at the beginning of each switching cycle, turns on when the inductor current $i_{\rm L}$ decreases to $i_{\rm vy}$, and remains in an on-state until the end of the present switching cycle.

For a practical switching dc–dc converter, as its switching frequency is usually much higher than the natural frequency of a low pass filter, the output voltage can be assumed to be constant.[9,10,17,23] In this case, the system becomes one-dimensional and the inductor current waveform becomes piecewise linear.

The one-dimensional discrete iterative map model of a PCM controlled switching dc–dc converter in CCM with ramp compensation was given as[9,10,17]

$$\begin{aligned} i_{n+1} &= i_n + m_1 T, \quad i_n \le I_{\rm bp}, \\ i_{n+1} &= -\frac{m_2 - m_{\rm c}}{m_1 + m_{\rm c}} i_n + \frac{m_1 + m_2}{m_1 + m_{\rm c}} I_{\rm pk} \\ &\quad - m_2 T, \quad i_n > I_{\rm bp}, \end{aligned} \tag{2}$$

where $I_{\rm bp} = I_{\rm pk} - (m_1 + m_{\rm c})T$ is defined as the value of $i_{\rm L}$ at the beginning of the clock pulse which reaches $i_{\rm pk}$ just at the end of the clock pulse as shown in Fig. 2(a), i_n and i_{n+1} are the inductor currents at the beginning of the n-th and the $(n+1)$-th clock pulses respectively, m_1 and m_2 are the increasing and decreasing slopes of inductor current of the switching dc–dc converter.

Figure 2(b) shows an illustration of a discrete iterative map model with ramp compensation for VCM control. In the same way, the one-dimensional discrete iterative map model of a VCM controlled switching dc–dc converter in CCM with ramp compensation can be obtained to be

$$\begin{aligned} i_{n+1} &= i_n - m_2 T, \quad i_n \ge I_{\rm bv}, \\ i_{n+1} &= -\frac{m_1 - m_{\rm c}}{m_2 + m_{\rm c}} i_n + \frac{m_1 + m_2}{m_2 + m_{\rm c}} I_{\rm vy} \\ &\quad + m_1 T, \quad i_n < I_{\rm bv}, \end{aligned} \tag{3}$$

where $I_{\rm bv} = I_{\rm vy} + (m_2 + m_{\rm c})T$ is defined as the value of $i_{\rm L}$ at the beginning of the clock pulse which reaches $i_{\rm vy}$ just at the end of the clock pulse.

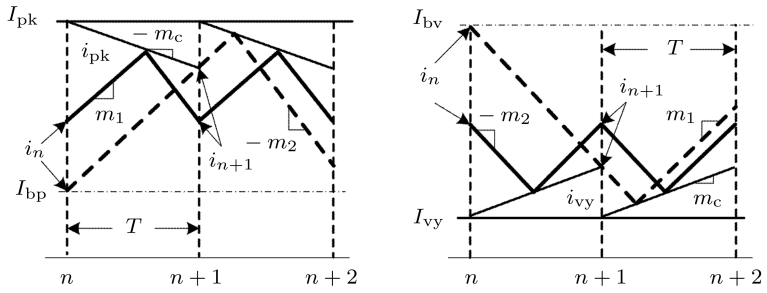


Fig. 2. Illustrations of a discrete iterative map model with ramp compensation for PCM control (a) and VCM control (b).

For three basic switching dc–dc converters, i.e. buck, boost, and buck-boost converters, m_1 and m_2 are given in Eqs. (4a), (4b), and (4c), respectively, as

$$\text{buck}: \quad m_1 = \frac{E - V_o}{L}, \quad m_2 = \frac{V_o}{L}; \tag{4a}$$

$$\text{boost}: \quad m_1 = \frac{E}{L}, \quad m_2 = \frac{V_o - E}{L}; \tag{4b}$$

$$\text{buck-boost}: \quad m_1 = \frac{E}{L}, \quad m_2 = \frac{V_o}{L}, \tag{4c}$$

where E and V_o are the input voltage and the output voltage respectively.

3. Operation regions with ramp compensation

3.1. Duty ratio range

For a PCM control, eigenvalue λ_p of the characteristic equation for the inner compensated loop was given as[9,10,17]

$$\lambda_p = -\frac{m_2 - m_c}{m_1 + m_c}. \tag{5}$$

To ensure stable operation, $|\lambda_p| < 1$ must be satisfied. With the consideration of inductor current volt-second balance in a steady state, we have $m_1 D = m_2(1 - D)$, where D is the duty ratio of the switching dc–dc converter in the steady-state. It is well known that without ramp compensation, the PCM controlled switching dc–dc converter is stable only when $D < 0.5$. In order to ensure stable operation for the PCM controlled switching dc–dc converter when $D \geq 0.5$, ramp compensation must be included and the slope of the compensation ramp must satisfy

$$m_c > m_{cp} = \frac{m_2 - m_1}{2}, \tag{6}$$

where m_{cp} is defined as the critical slope of the compensation ramp for the PCM control. In particular, period-doubling occurs when $\lambda_p = -1$.[17] Hence, m_{cp} can also be obtained by substituting $\lambda_p = -1$ into Eq. (5).

From inequality (6) with the adoption of ramp compensation, the critical duty ratio D_{cp} for the stable operation of the PCM controlled switching dc–dc converter when $D \geq 0.5$ then becomes

$$D_{cp} = 0.5 + \Delta D_p = 0.5 + 0.5 k_p/(1 + k_p), \tag{7}$$

where $k_p = m_c/m_1$ is defined as the slope-compensation-factor (SCF) for the PCM control and ΔD_p is the corresponding duty ratio margin. According to the previous discussion, it is known that the critical duty ratio is the period-doubling bifurcation point.

For VCM control, it is clear that $i_n \geq I_{bv}$ does not exist in stable period-one operation. The stability of the switching dc–dc converter is affected only when $i_n < I_{bv}$. The eigenvalue λ_v of the characteristic equation of Eq. (3) is given by

$$\lambda_v = -\frac{m_1 - m_c}{m_2 + m_c}. \tag{8}$$

To ensure stable operation, $|\lambda_v| < 1$ must be satisfied. Therefore, the VCM controlled switching dc–dc converter without ramp compensation is stable only when $D > 0.5$. In order to ensure stable operation for the VCM controlled switching dc–dc converter when $D \leq 0.5$, ramp compensation must be included and the slope of the compensation ramp must satisfy

$$m_c > m_{cv} = \frac{m_1 - m_2}{2}, \tag{9}$$

where m_{cv} is defined as the critical slope of the compensation ramp for VCM control. Similarly, the critical duty ratio D_{cv} for stable operation of the VCM controlled switching dc–dc converter when $D \leq 0.5$ then becomes

$$D_{cv} = 0.5 - \Delta D_v = 0.5 - 0.5 k_v/(1 + k_v), \tag{10}$$

where $k_{\rm v} = m_{\rm c}/m_2$ is defined as SCF for the VCM control and $\Delta D_{\rm v}$ is the corresponding duty ratio margin.

From expressions (6), (7), (9), and (10), and $m_1 D = m_2(1-D)$, the critical duty ratio can be deduced to be a function of $m_{\rm c}$ and D. Figures 3(a) and 3(b) show the relations between critical duty ratio and duty ratio for the PCM control and the VCM control respectively, from which it can be known that the critical duty ratios $D_{\rm cp}$ and $D_{\rm cv}$ are 0.5 without ramp compensation, and $D_{\rm cp}$ and $D_{\rm cv}$ equal D with critical ramp compensations $m_{\rm cp}$ and $m_{\rm cv}$.

As shown in Fig. 3(a), $D_{\rm cp}$ is larger than D when $m_{\rm c} > m_{\rm cp}$, which means that the PCM controlled switching dc–dc converter is stable when $D \geq 0.5$. As shown in Fig. 3(b), $D_{\rm cv}$ is smaller than D when $m_{\rm c} > m_{\rm cv}$, which means that the VCM controlled switching dc–dc converter is stable when $D \leq 0.5$. With $m_{\rm c}$ further increasing, i.e. $m_{\rm c} = 2m_{\rm cp}$, $3m_{\rm cp}$ and so on for the PCM control and $m_{\rm c} = 2m_{\rm cv}$, $3m_{\rm cv}$ and so on for the VCM control, the corresponding duty ratio margins $\Delta D_{\rm p}$ and $\Delta D_{\rm v}$ gradually increase, which means that the ramp compensation further extends stable operation ranges to $D \geq 0.5$ for PCM control and to $D \leq 0.5$ for VCM control separately.

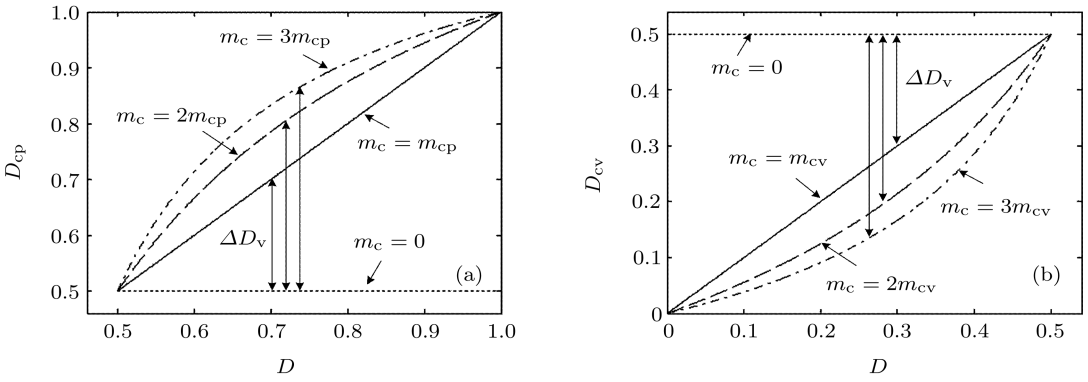
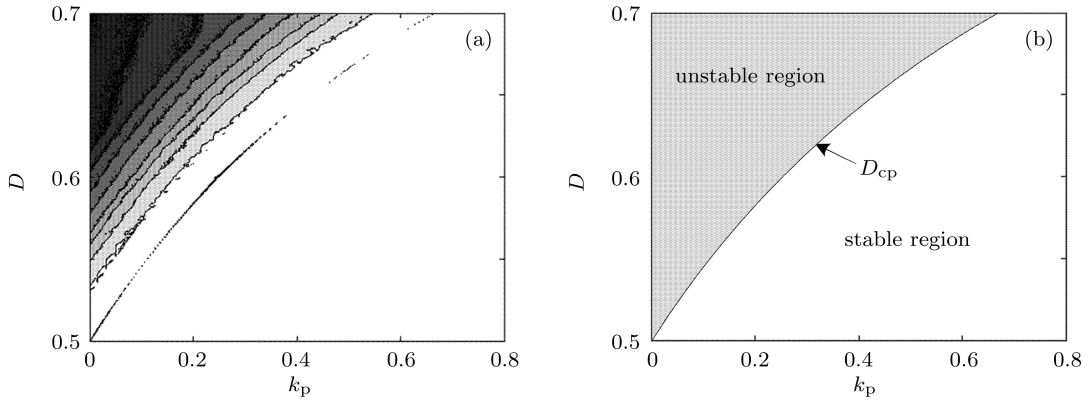


Fig. 3. Relations between critical duty ratio and duty ratio for PCM control (a) and VCM control (b).

3.2. Parameter space maps and operation regions

With circuit parameter variation ranges, i.e. $D = 0.5$–0.7 and $k_{\rm p} = 0$–0.8 for the PCM control, and $D = 0.3$–0.5 and $k_{\rm v} = 0$–0.8 for the VCM control, parameter space maps of Eqs. (2) and (3), i.e. two-dimensional dynamical behaviour distribution maps, can be obtained as shown in Figs. 4(a) and 4(c), which depict their asymptotic behaviours with colours over a grid of the parameter space. In Figs. 4(a) and 4(c), the higher periodicities are depicted with darker grey levels, where the white area means low period and the darkest shade implies chaos. According to Eqs. (7) and (10), Figures 4(b) and 4(d) show the corresponding operation regions of the orbit states in Figs. 4(a) and 4(c).



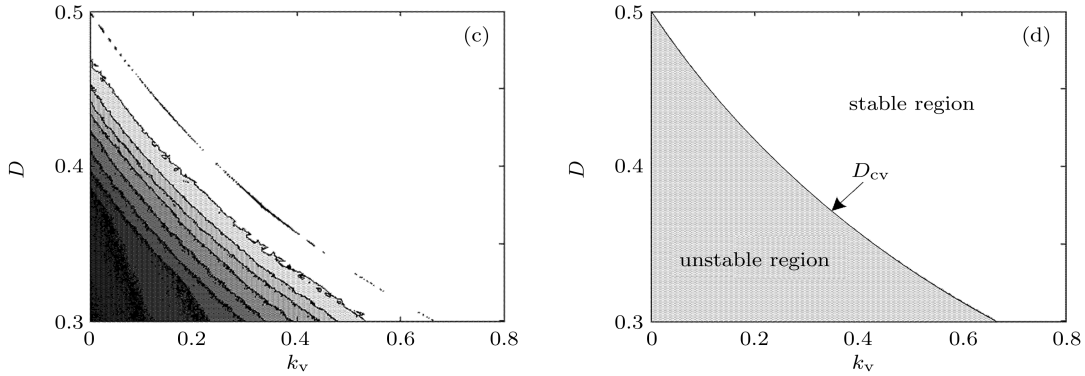


Fig. 4. Parameter space maps for PCM control (a) and VCM control (c) and their operation regions (b) and (d), respectively, corresponding to (a) and (c).

Line D_{cp} in Fig. 4(b) and line D_{cv} in Fig. 4(d) are obtained from Eqs. (7) and (10) respectively. Line D_{cp} is the period-doubling bifurcation borderline for the PCM control, and the region below line D_{cp} is stable, while the region above line D_{cp} consists of regions of unstable low period and chaos. Line D_{cv} is the period-doubling bifurcation borderline for the VCM control, and the region above line D_{cv} is stable, while the region below line D_{cv} is composed of regions of unstable low period and chaos. From Fig. 4, it can be clearly known that the stable operation regions between PCM and VCM controlled switching dc–dc converters are symmetrical and the stable operation regions gradually extend with the increase of SCF.

4. Symmetrical dynamics

Based on the discrete iterative maps given in Eqs. (2) and (3), when circuit parameters are kept constant, i.e. $E = 12$ V, $I_{pk} = 1.5$ A, $I_{vy} = 0.8$ A, $L = 0.6$ mH, and $T = 50$ μs while D varies from 0.3 to 0.7, bifurcation diagrams of inductor currents and their corresponding Lyapunov exponent spectra of PCM and VCM controlled buck converters with $k_p = 0$ and $k_v = 0$ are shown in Fig. 5. Note that for the buck converter, $V_o = DE$, and the values of m_1 and m_2 can be obtained from Eq. 4(a).

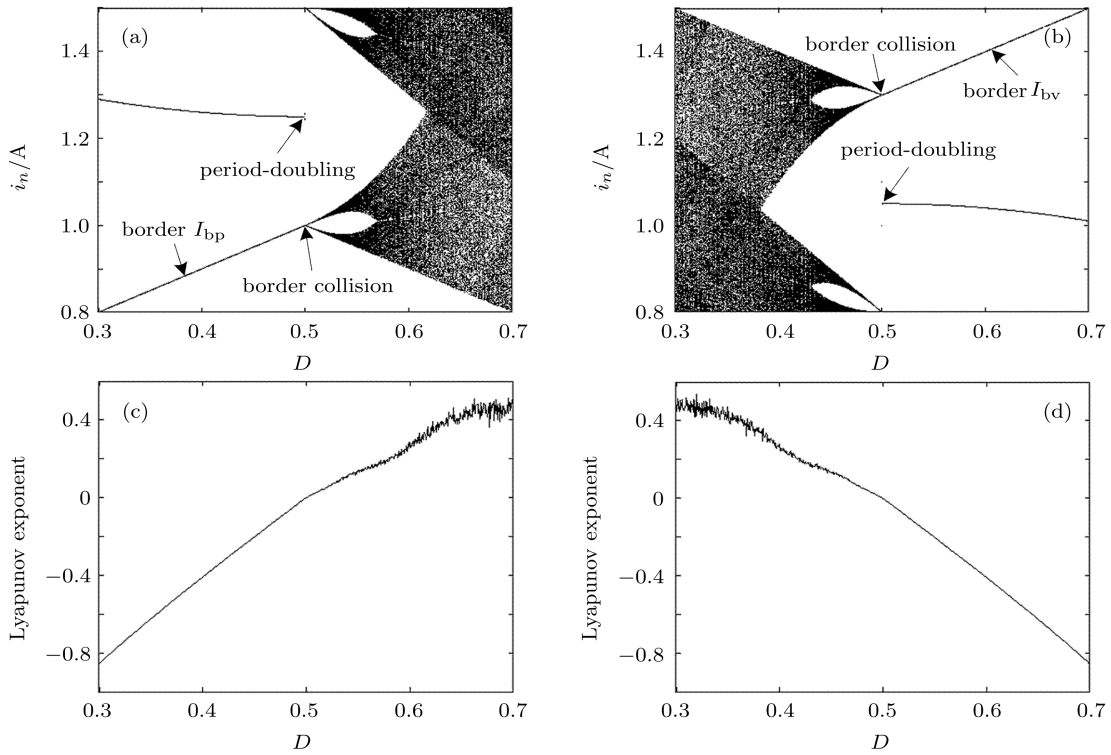


Fig. 5. Bifurcation diagrams for PCM control (a) and VCM control (b) and their Lyapunov exponent spectra (c) and (d), respectively, corresponding to (a) and (b), with D used as a parameter.

As shown in Fig. 5(a), the PCM controlled buck converter has a non-inverse period-doubling route to chaos with the increase of D, where period-doubling bifurcation occurs when $D = 0.5$. At the period-doubling bifurcation point, the system orbit collides with the borderline $I_{\rm bp}$, resulting in border collision bifurcation. Following the border collision, a chaotic orbit develops, and with D increasing further, the pieces of the attractor are joined pairwise into a one-piece attractor.

As shown in Fig. 5(b), the VCM controlled buck converter has an inverse period-doubling route to chaos with the increase of D, where period-doubling bifurcation occurs when $D = 0.5$ and the border collision bifurcation occurs when the system orbit collides with the borderline $I_{\rm bv}$ at the same parameter value.

Figures 5(c) and 5(d) show the Lyapunov exponents corresponding to Figs. 5(a) and 5(b) respectively. From Figs. 5(a) and 5(c), it can be known that when D increases to $D = 0.5$, period-doubling bifurcation occurs and the Lyapunov exponent simultaneously increases to zero.

From Figs. 5(a) and 5(b), it is found that bifurcation diagrams of PCM and VCM controlled switching dc–dc converters exhibit symmetry and have a symmetrical point at (0.5, 1.125 A). This symmetrical point is the intersection point of axis $D = 0.5$ and $i_n = (I_{\rm pk} + I_{\rm vy})/2$. It is found that the Lyapunov exponent spectra of Figs. 5(c) and 5(d) also exhibit symmetry and have a symmetrical axis at $D = 0.5$, which is in accordance with the symmetrical point of the corresponding bifurcation diagrams of Figs. 5(a) and 5(b).

According to the discrete iterative maps of Eqs. (2) and (3), with the same circuit parameters as those in Fig. 5, and letting $k_{\rm p} = 0.2$ and $k_{\rm v} = 0.2$, the inductor current bifurcation diagrams of PCM and VCM controlled buck converters are shown in Figs. 6(a) and 6(b) respectively.

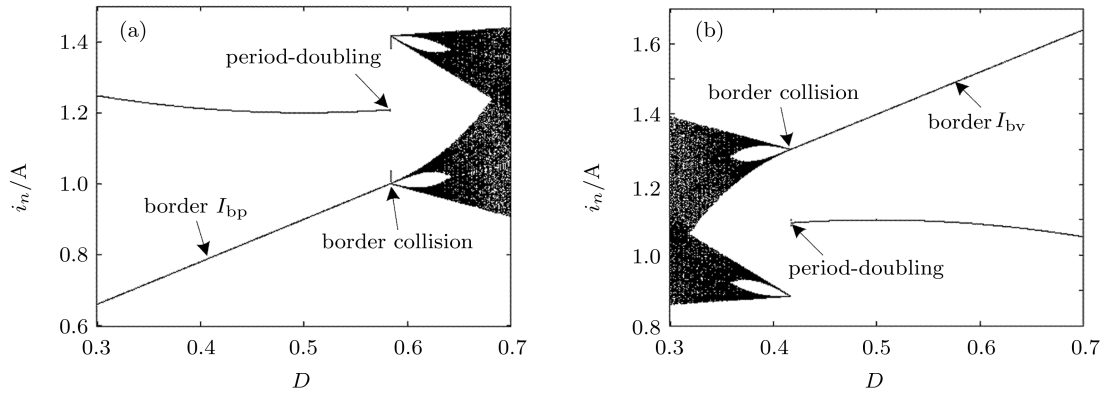


Fig. 6. Bifurcation diagrams for PCM control with $k_{\rm p} = 0.2$ (a) and VCM control with $k_{\rm v} = 0.2$ (b).

Comparing Fig. 6(a) with Fig. 5(a), it is found that the period-doubling bifurcation and border collision bifurcation points shift toward large values of D due to the adoption of ramp compensation, which means that the stable operation region becomes wider. With $k_{\rm p} = 0.2$, the duty ratio margin $\Delta D_{\rm p} = 0.083$ and the corresponding critical duty ratio $D_{\rm cp} = 0.583$ can be obtained from Eq. (7). It is observed that period-doubling bifurcation occurs when $D = 0.583$ in Fig. 6(a), which coincides well with the case $D_{\rm cp} = 0.583$ calculated from Eq. (7). With $k_{\rm v} = 0.2$, the duty ratio margin $\Delta D_{\rm v} = 0.083$ and the corresponding critical duty ratio $D_{\rm cv} = 0.417$ can be obtained from Eq. (10). It is observed that period-doubling bifurcation occurs when $D = 0.417$ in Fig. 6(b), which accords well with the case $D_{\rm cv} = 0.417$ calculated from Eq. (10).

Comparing Fig. 6(a) with Fig. 6(b), it is also found that the bifurcation diagrams of PCM control and VCM control have a symmetrical point at (0.5, 1.125 A) due to the adoption of ramp compensation, which means that ramp compensation does not affect the symmetry existing in PCM and VCM controlled switching dc–dc converters.

To further study the symmetrical dynamical behaviours of PCM and VCM controlled switching dc–dc converters by utilizing ramp compensation, figures 7(a) and 7(b) show bifurcation diagrams for PCM control when $D = 0.7$ and for VCM control when $D = 0.3$ respectively, with SCF used as a parameter.

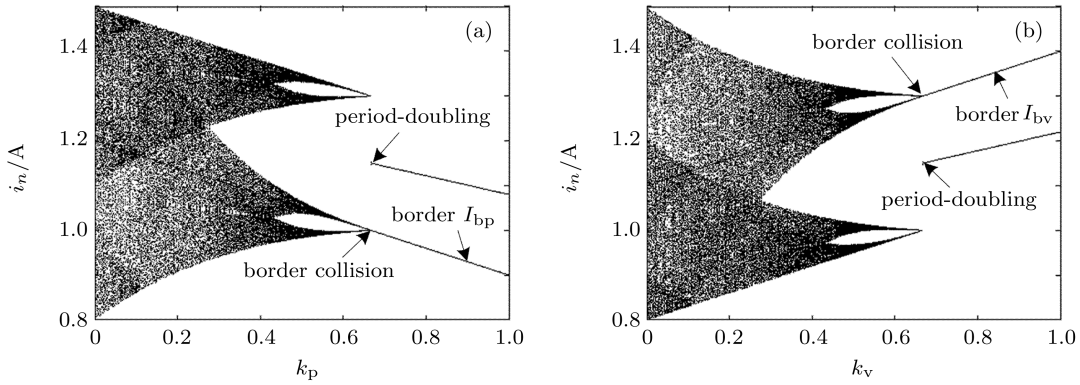


Fig. 7. Bifurcation diagrams for PCM control when $D = 0.7$ and $k_{\rm p} = 0$–1 (a) and for VCM control when $D = 0.3$ and $k_{\rm p} = 0$–1 (b), with SCF used as a parameter.

It can be observed that with the increase of SCF, period-doubling bifurcations occur when $k_{\rm p} = 0.67$ and $k_{\rm v} = 0.67$, which accords well with the results calculated from Eqs. (7) and (10) respectively. Before the period-doubling bifurcations, border collision bifurcations occur since fixed points of the switching dc–dc converter collide with the borderlines $I_{\rm bp}$ and $I_{\rm bv}$ separating two smooth regions. Observed from Figs. 7(a) and 7(b), the bifurcation diagrams of PCM control and VCM control with SCF as a parameter have a symmetrical axis $i_n = (I_{\rm pk} + I_{\rm vy})/2$.

5. Experimental results

To verify the symmetrical dynamical phenomena between PCM and VCM controlled switching dc–dc converters and the extension of the stable operation region due to the adoption of ramp compensation, experimental studies on the buck converter are performed with $D = 0.51$ for PCM control, and $D = 0.49$ for VCM control. The experimental results are shown in Fig. 8.

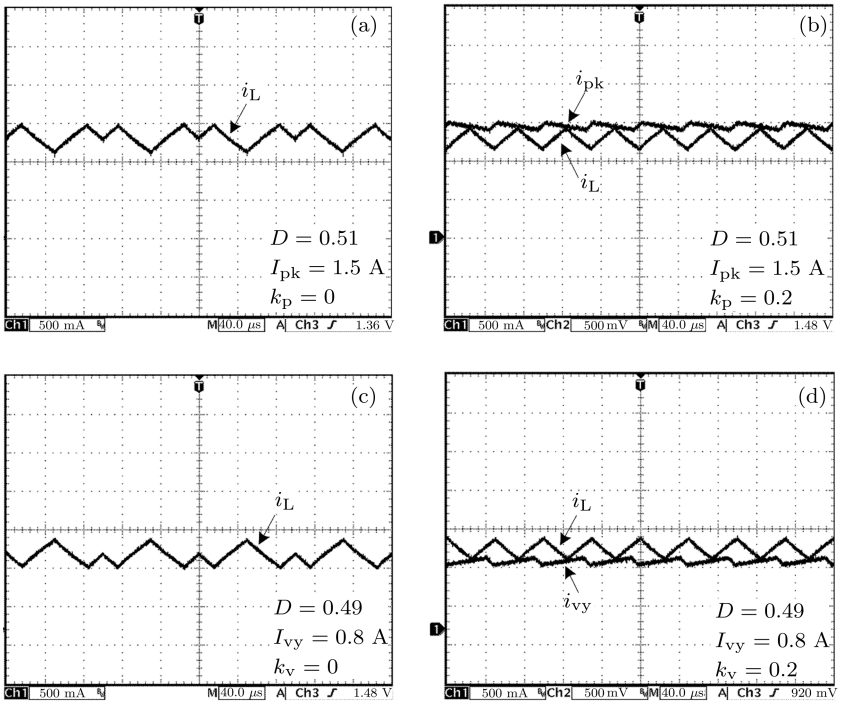


Fig. 8. Experimental results for PCM control with $k_{\rm p} = 0$ (a) and $k_{\rm p} = 0.2$ (b) and for VCM control with $k_{\rm v} = 0$ (c) and $k_{\rm v} = 0.2$ (d) separately.

Figures 8(a) and 8(c) show inductor current experimental waveforms of PCM and VCM controlled buck converters without ramp compensation respectively, from which symmetrical period-2 waveforms can be observed. Figures 8(b) and 8(d) show inductor current experimental waveforms of PCM control with $k_{\rm p} = 0.2$ and VCM control with $k_{\rm v} = 0.2$ respectively, where symmetrical stable period-1 waveforms can be observed, which demonstrates that the compensation ramp extends the stable region and does not affect the symmetrical dynamics of PCM and VCM controlled switching dc–dc converters. The experimental results verify the analysis results and simulation results obtained in this paper.

6. Conclusions

One-dimensional iterative map models of PCM and VCM controlled switching dc–dc converters with ramp compensation are established. Based on the iterative map model and eigenvalue of the corresponding characteristic equation, non-inverse and inverse bifurcation diagrams and the Lyapunov exponent spectra of PCM control and VCM control with duty ratio as a parameter are obtained. The dynamical behaviours of switching dc–dc converters with ramp compensation are investigated by using the operation region, parameter space map, bifurcation diagram, and Lyapunov exponent spectrum. It is concluded that the ramp compensation can extend the stable operation ranges to $D > 0.5$ for PCM control and to $D < 0.5$ for VCM control separately. In particular, the research results indicate that PCM and VCM controlled switching dc–dc converters have symmetrical dynamical behaviours corresponding to a symmetrical point and symmetrical axis. Experimental results are given to verify the analysis results and simulation results.

References

[1] Maity S, Tripathy D, Bhattacharya T K and Banerjee S 2007 *IEEE Trans. Circuit Syst.* I **54** 1120

[2] Wang F Q, Zhang H and Ma X K 2008 *Acta Phys. Sin.* **57** 1522 (in Chinese)

[3] Zhang X T, Ma X K and Zhang H 2008 *Acta Phys. Sin.* **57** 6174 (in Chinese)

[4] Wang X M, Zhang B and Qiu D Y 2008 *Acta Phys. Sin.* **57** 2728 (in Chinese)

[5] Yang R, Zhang B and Zhu L L 2008 *Acta Phys. Sin.* **57** 2770 (in Chinese)

[6] Aroudi A E, Benadero L, Toribio E and Olivar G 1999 *IEEE Trans. Circuits Syst.* I **46** 1374

[7] Chan W C Y and Tse C K 1997 *IEEE Trans. Circuits Syst.* I **44** 1129

[8] Banerjee S, Parui S and Gupta A 2004 *IEEE Trans. Circuits Syst.* II **51** 649

[9] Bao B C, Xu J P and Liu Z 2009 *Acta Phys. Sin.* **58** 2949 (in Chinese)

[10] Bao B C, Xu J P and Liu Z 2009 *Chin. Phys.* B **18** 4742

[11] Zou J L and Ma X K 2008 *Acta Phys. Sin.* **57** 720 (in Chinese)

[12] Kavitha A and Uma G 2008 *IEEE Trans. Power Electron.* **23** 2878

[13] Mazumder S K, Nayfeh A H and Boroyevich D 2001 *IEEE Trans. Power Electron.* **16** 201

[14] Zhou Y F, Chen J N, Iu H H C and Tse C K 2008 *Int. J. Bifurc. Chaos* **18** 121

[15] Zhusubaliyev Z T, Soukhoterin E A and Mosekilde E 2003 *IEEE Trans. Circuits Syst.* I **50** 1047

[16] Wong S C, Tse C K and Tam K C 2004 *Int. J. Bifurc. Chaos* **14** 2971

[17] Bao B C, Xu J P and Liu Z 2008 *J. University of Electronic Science and Technology of China* **37** 397 (in Chinese)

[18] Banerjee S, Parui S and Gupta A 2004 *IEEE Trans. Circuits Syst.* II **51** 649

[19] Zhao Y B, Zhang D Y and Zhang C J 2007 *Chin. Phys.* **16** 933

[20] Wang X M, Zhang B, Qiu D Y and Chen L G 2008 *Acta Phys. Sin.* **57** 6112 (in Chinese)

[21] Zhou Y F, Chen J N, Tse C K, Ke D M, Shi L X and Sun W F 2004 *Acta Phys. Sin.* **53** 3676 (in Chinese)

[22] Zhou G H, Bao B C, Xu J P and Jin Y Y 2010 *Chin. Phys.* B **19** 050509

[23] Zhou G H, Xu J P and Bao B C 2010 *Acta Phys. Sin.* **59** 2272 (in Chinese)